Real-Time Iris Detection on Coronal-Axis-Rotated Faces

Claudio A. Perez, *Senior Member, IEEE*, Vanel A. Lazcano, and Pablo A. Estévez, *Senior Member, IEEE*

***Abstract*—Real-time face and iris detection on video sequences is important in diverse applications such as, study of the eye function, drowsiness detection, virtual keyboard interfaces, face recognition, and multimedia retrieval. In this paper, a real-time robust method is developed to detect irises on faces with coronal axis rotation within the normal range of -40° to 40°. The method allows head movements with no restrictions to the background. The method is based on anthropometric templates applied to detect the face and eyes. The templates use key features of the face such as the elliptical shape, and location of the eyebrows, nose, and lips. For iris detection, a template following the iris–sclera boundary shape is used. The method was compared to Maio–Maltoni's and Rowley's methods for face detection on five video sequences (TEST 1). The method was also assessed in an additional set of five video sequences for iris detection (TEST 2). Results of correct face detection in TEST 1 were above 99% in three of the five video sequences. The fourth video sequence reached 97.6% and the third 90.6%. In TEST 2, the iris detection was above 96% in all five video sequences with two above 99.7% and two at 100%. Face size estimation is also above 99.9%. The average processing time of our method was 0.02 s per frame. Thus, the proposed method can process frames at a rate near to 50 frames/s, and therefore, is applicable in real time in a standard personal computer (PC 1.8 GHz).**

***Index Terms*—Anthropometric templates, face rotation, iris tracking, real-time face detection, real-time iris detection.**

I. Introduction

GAZE estimation represents an important area of research in human–machine interfaces. Through eye gaze estimation, the observer's fixation point can be determined and followed. Interfaces have been proposed to activate or command devices by eye gaze [9], [30], [31]. Other applications have been developed for drowsiness detection [7], [8], to aid handicapped individuals [6], [14], or to operate a virtual computer keyboard by detecting eye position [23]. New applications for devices controlled by eye gaze are being considered in complex technological environments, such as hospital operating rooms, airplane cockpits, and industrial control units [13], [21], [30]. Interaction with the computer through eye gaze ideally involves passive sensing of human eye position, and therefore, eye tracking methods should be noninvasive, fast, and robust [31].

Many eye tracking methods are invasive or partially invasive. Eye tracking methods have been based on devices mounted on helmets, electrodes that measure the activity of the eyeball, light reflected by the cornea (punkinje images), or near-infrared (NIR) imaging [4], [5], [33]. Lately, video cameras have been used as an alternative automated method for monitoring eye movements in a nonintrusive manner.

Many noninvasive methods for eye gaze estimation need the face position first. Face position estimation is a very important problem in the field of computer vision [32]. Several methods have been developed for this problem using NIR [4], [33], neural networks [25], [28], [29], skin color [11], [31], and templates [10], [16], [19]. Neural-network-based methods have been used to recognize [24] and detect faces [28], [29]. In [28], a 20×20 window is used to scan the input image looking for faces in different resolutions. The output goes to a neural network of 400 inputs and 36 outputs to detect a rotation angle. The method is computationally intensive in training and processing time, because the scanning is performed over the complete image [18].

Methods based on skin color to detect faces use the color space to find a skin cluster. In addition, with some heuristic rules these methods are able to detect faces in real time with a good performance [1]. Jones [12] presents a procedure to determine the color skin distribution and non-skin distribution in a huge image database with a good performance. Nevertheless, color-based methods may be restricted to specific ethnic groups or may fail under varying illumination conditions.

The main limitations of noninvasive methods for face and eye detection are that they: 1) assume homogeneous background [15]; 2) focus on only one eye and therefore do not follow head movements or follow very small head movements [30]; and 3) fail to detect eyes while blinking or require manual initialization. Besides, some methods impose restrictions such as symmetry that limits the background content. Other methods for face detection impose some restrictions on the background color. Methods for eye tracking that rely on an image zoomed into one eye may not be applicable to standard images where the eyes fit in a few dozens of pixels. Some applications are restricted to open eyes, and others fail when eyes are wide open [30]. It is also acknowledged that most developed methods have been tested in a laboratory with a rather small set of images. It is apparent that most of the face and eye tracking methods are far from being applicable in real time on a standard personal computer.

In this paper, a new method is proposed for real-time iris detection on faces that can move within the field of view of the camera, and can rotate around the coronal axis. The method uses anthropometric data about faces and eyes to guide the face and eye detection algorithm, thus, limiting the number of computations to allow real-time processing. Three different templates are built to allow face detection, limit the eye search region,

Manuscript received February 7, 2005; revised August 5, 2006. This work was supported in part by the CONICYT-Chile under Project FONDECYT 1040693 and in part by the Department of Electrical Engineering, Universidad de Chile. This paper was recommended by Associate Editor L. Zang.

The authors are with the Department of Electrical Engineering, University of Chile, Santiago, Chile (e-mail: clperez@ing.uchile.cl; vlazcano@ing.uchile.cl; pestevez@ing.uchile.cl).

Digital Object Identifier 10.1109/TSMCC.2007.900647

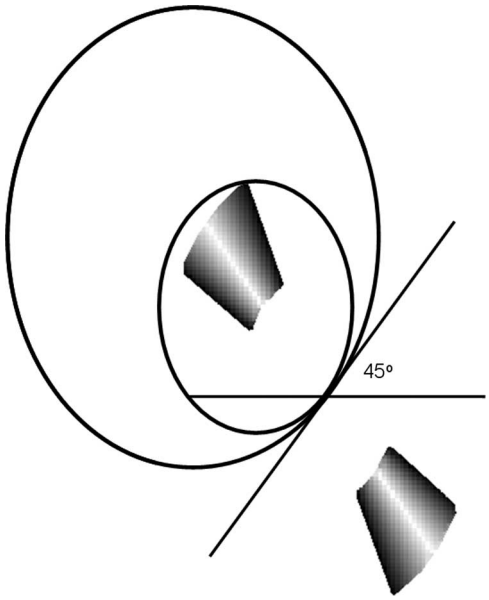

Fig. 1. Template for a vector at an angle of 45° used in the coarse face detection. It shows the locus for the center of all possible ellipses tangent to the vector at an angle of 45°. As an example, it shows the largest and smallest possible ellipses for that template.

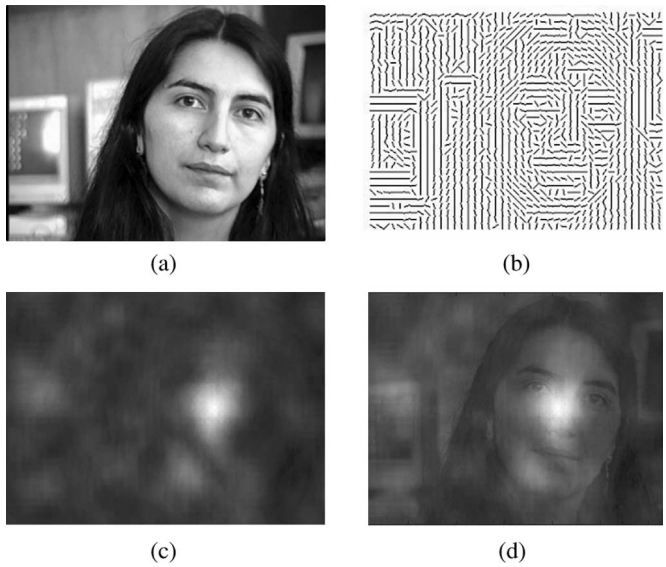

Fig. 2. Example of the coarse face detection stage. (a) Original image, (b) coarse directional image, (c) accumulator, and (d) superposition of the accumulator and original image.

and allow detection of the iris–sclera boundary. The coarse face detection stage uses the face detection approach previously proposed by Maio and Maltoni [19] but incorporates the following new aspects. Templates are built to consider rotated faces in the coronal axis. A template to detect the most probable region for the eye's location within the face is developed based on measurements made on a frontal face database. A ratio between two line integrals over a semicircular template is developed to detect the iris–sclera boundary. Preliminary results for different parts of the proposed method were previously presented in [22], [26], and [27].

II. Methodology

The proposed method for iris tracking in rotated faces is an extension of a method previously developed by Maio and Maltoni to detect only faces [19]. Our method is built into three stages requiring only gray level information, and solves the restrictions of other methods mentioned in the introduction. The three stages are: coarse face detection, fine face detection, and iris detection.

A. Coarse Face Detection

The goal of this stage is to find the approximate face location within the image. In [19], the Hough transform is used in this stage. A directional image I_D is computed, and then, this directional image is scanned with a set of elliptical templates. Each tangent vector in the directional image may be associated with 36 elliptical templates. The method works for face sizes that fit with ellipses that have major axis radius between 60–120 pixels. For a particular vector of 45° in the coarse directional image, Fig. 1 shows the corresponding templates for the center of all possible ellipses that will be tangent to that vector. The cone sections in gray levels show the locus for the centers of all possible ellipses tangent to the vector in 45°. It also shows the maximum and minimum possible ellipses for the template. These ellipses represent the limits for the face size detection. The method is not directly applicable to sagital face rotations. The templates score all possible centers with tangent vectors in the directional image in an accumulator. After scanning the entire directional image, the highest score in the accumulator is taken as the most probable center of the ellipse where the face is located. Fig. 2 shows the coarse face detection stage for a face with approximately $-10°$ coronal rotation. Fig. 2(a) shows the original image, (b) the directional image, (c) the accumulator, and (d) the superposition of the original image and the accumulator.

B. Fine Face Detection

This stage is designed to detect the face location determining the face rotation angle and size.

1) High-Resolution Directional Image: A high-resolution directional image I_{HRD} is computed using neighborhoods of 3×3 pixels according to the method developed in [19].

2) Region of Interest in I_{HRD}: In I_{HRD}, the face search is reduced to a small region around the most probable face center determined in the coarse face detection. Therefore, the region of interest I_{ROI} for the face search in I_{HRD} satisfies

$$I_{\mathrm{ROI}} = \left\{ I_{\mathrm{HRD}}(i,j) / \mathrm{abs}(i - i_0) \leq \frac{h_v}{2};\ \mathrm{abs}(j - j_0) \leq \frac{h_v}{2} \right\} \tag{1}$$

where (i_0, j_0) are the coarse center coordinates and h_v is the maximum semiaxis of a vertical ellipse detectable in the image.

3) Creation of Face Template for Fine Face Detection: Face templates were created offline and stored for online detection.

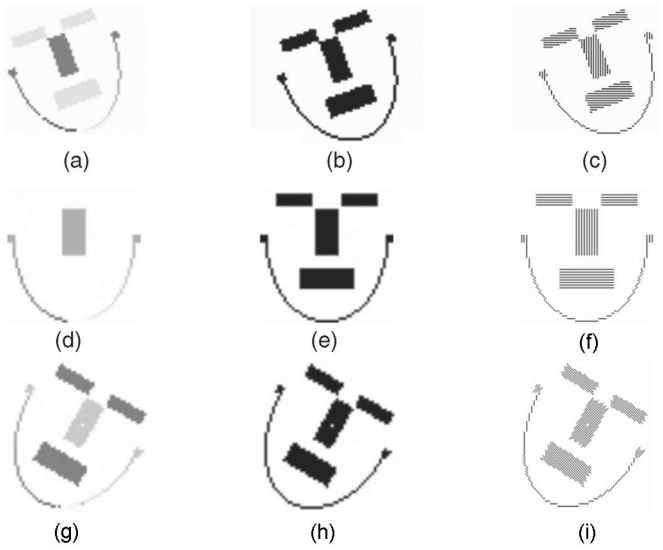

Fig. 3. Template construction for different rotation angles: (a), (d), and (g) show the angle in gray level; (b), (e), and (h) show the module; and (c), (f) and (i) show the final template.

Templates were created for each size r and for each rotation angle ϕ. Let R be the set of different values for r, such that

$$R = \{r/b_{\min} \leq r \leq b_{\max}\} \tag{2}$$

and $\mathbf{\Phi}$ is the set of different values for ϕ, such that

$$\Phi = \{\phi/\phi_{\min} \leq \phi \leq \phi_{\max}\}. \tag{3}$$

$T_{FR\Phi}$ is an array that stores all the templates for different sizes and angles. These templates are used in the fine face detection, performing a line integral along the template over the I_{ROI} in I_{HRD}. The $T_{FR\Phi}$ was created over an ellipse resembling the face shape. The $T_{FR\Phi}$ complies with the following: by setting $b_{\min} = 60$ and $b_{\max} = 120$, a total of 21 different size ellipses, with a step of three pixels, for each rotation angle were considered. The rotation angle was considered varying in steps of 10° from $\phi_{\min} = -40°$ to $\phi_{\max} = 40°$, and therefore, a total of 21×9 templates were built.

Only the lower half of the face elliptical contour was considered for the $T_{FR\Phi}$. Distinctive anatomical elements in the face region are: eyebrows, nose, lips, and location of the tragus in the auricle. Vectors in the directional image associated to these four anatomical elements follow similar patterns across the population. Anthropometric templates were built on the face elliptical contour plotting the limits to the nearest integer of the average plus and minus the standard deviation for each anatomical element as shown in Fig. 3.

The angle φ between the neighborhood of the points in the elliptical template and the center of the ellipse is calculated. The average of these angles $\bar{\theta}$ is obtained for each neighborhood of the elliptical contour and the tangent to the neighborhood in I_{HRD} scale is calculated by

$$\varphi = a\tan\left(-\frac{1}{A_r \tan(\bar{\theta})}\right) \tag{4}$$

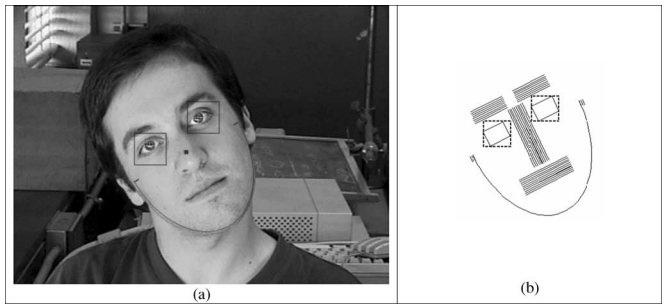

Fig. 4. (a) Face with coronal rotation of approximately 30°. An elliptical contour is fit to the mandibular and chin region. (b) Corresponding face template with directional information also with approximately 30° coronal rotation.

where $A_r = b/a$ is the face aspect ratio. This aspect ratio is defined as the ratio between the minor axis b and major axis a, of an ellipse fitting the face as shown in Fig. 4(a). The angles in the face template are defined as follows: the eyebrows and mouth tend to be horizontal (0°) and the nose and tragus tend to be vertical (90°). These angles are measured relative to a frontal face with no coronal rotation. The angles were assigned to each point of the face anatomical elements according to the corresponding angles in I_D. These angles were measured in the directional images of the AR Face database [20]. For faces with coronal rotation in angle ϕ, the angles in the template are: ϕ for the eyebrows and mouth, and $90° - \phi$ for the nose and tragus.

Fig. 4(a) shows a face with coronal rotation of approximately 30°. An elliptical contour is fit to the mandibular and chin region to show how the face can be represented by an ellipse. The aspect ratio of the ellipse is the same as that of the face. Fig. 4(b) shows a face template also rotated by approximately 30°. The directional information for the eyebrow, nose, and mouth region is also shown on the template.

Fig. 3(a), (d), and (g) shows the angles associated to each pixel of the template in gray level. White level is used for 0°, black level for 180°, and gray levels for angles in between. Fig. 3(b), (e), and (h) shows the magnitude of the templates with black representing 255 and white 0. Fig. 3(c), (f), and (i) shows the final $T_{FR\Phi}$ for rotation of −40°, 0°, and 40°, respectively. These $T_{FR\Phi}$ include the elliptical face contour and the anatomical elements identified with rectangular marks representing the eyebrows, nose, mouth, and tragus.

4) Fine Detection: The $T_{FR\Phi}$ is used to measure its similarity with I_{ROI}. A discrete and normalized line integral $I_{T_{FR\Phi}}$, is performed on I_{ROI} for each possible value of the vertical semiaxis in the set formed by $[b_{\min}, \ldots, b_{\max}] \times [\phi_{\min}, \ldots, \phi_{\max}]$ according to

$$I_{T_{FR\Phi}}(i_o, j_o) = \frac{\sum_{i,j \in T_{FR\Phi}(i_0,j_0)} [I_{\mathrm{ROI}}(i,j)a(i,j) - (1 - I_{\mathrm{ROI}}(i,j))90]}{N_{T_{FR\Phi}}} \tag{5}$$

where $T_{FR\Phi}(i_0, j_0)$ is the template associated with semiaxis R and rotation angle Φ, centered at (i_0, j_0), and $a(i,j)$ is given by

$$a(i,j) = 90 - 2\min(|AT(i,j) - AI_R(i,j)|, 180 - |AT(i,j) - AI_R(i,j)|) \tag{6}$$

and, $N_{T_{FR\Phi}}$ is the number of pixels that belong to the template $T_{FR\Phi}$, $AT(i,j)$ is the angle associated to (i,j) in $T_{FR\Phi}$, and $AI_R(i,j)$ is the angle associated to (i,j) in I_{ROI}. The division by $N_{T_{FR\Phi}}$ allows normalization of the results relative to the size of the template. The factor $a(i,j)$ takes into account the disparity between the angle of $T_{FR\Phi}$ and I_{ROI}. For larger disparity angles, the line integral values are smaller. Therefore, the probability of choosing $T_{FR\Phi}$ as the best one to fit the face position in I_{ROI} decreases. The term calculating angular disparity as the minimum between $|AT(i,j) - AI_R(i,j)|$ and $180 - |AT(i,j) - AI_R(i,j)|$ allows to obtain their effective angle difference instead of calculating the inner or external angle. The line integral given in (5) is calculated using the $T_{FR\Phi}$ centered at all points (i_0, j_0) belonging to a 7×7 square neighborhood around the coarse-face-detected center. This calculation allows finding the best face location around the coarse-detected position. The template position center that maximizes $I_{T_{FR\Phi}}$ is designated as the position for the face center, and its vertical semiaxis defines the face size.

C. Iris Detection

The eyes' relative location within the face limits was measured in the AR Face database [20] to create generic templates. Four limits for the eyes were determined using the ear tragus as a reference point representing the middle of the face and the chin representing the face bottom limit. The four eye limits were the upper and lower eyelid limits, and the external and internal corners. The region delimited by these measurements represents $I_{er}(i,j)$, and therefore, a template was built with these values. Thus, once the fine face location has been performed, $I_{er}(i,j)$ is automatically determined. The regions where the eyes are located maintain their relative position in rotated templates. The templates are rotated in angle ϕ, and are created only once (offline) and stored for later use.

Once the $I_{er}(i,j)$ has been determined, the position of the iris is detected by first eliminating the bright reflections on the pupil or iris present in most eye images. A minimum filter within a 7 $\times$7 window is applied to eliminate reflections in $I_{er}(i,j)$.

Although the iris presents a circular shape in frontal faces, it is often occluded by the eyelids. The intersection of the iris outer boundary and the eyelids create angles α and β with respect to the horizontal [22]. These angles decrease up to 0° during blinking or when eyes are closed. Templates $T_{IR\Phi}$ were created, representing the edge between the iris and the sclera. Examining the frontal faces from the AR Face database, the average value found for angles α and β were 50° and 70°, respectively. We considered a rotation angle ϕ to correct the iris template for coronal face rotation.

The algorithm developed for iris detection uses the fact that there is high contrast between the iris and the sclera region, and that the iris is approximately circular. A ratio is calculated between two line integrals around a $T_{IR\Phi}$: one within and the other outside the iris [22]. This method is based on that proposed in [2]. A recent review in iris recognition is provided in [3]. In this paper, a ratio between both line integrals is proposed. Also, the line integrals are computed only between the angles that are not occluded by the eyelids considering $\alpha = 50°$ and $\beta = 70°$ as shown in Fig. 5. The ratio between the line integrals $R_{LI\Phi}$ in discrete form is

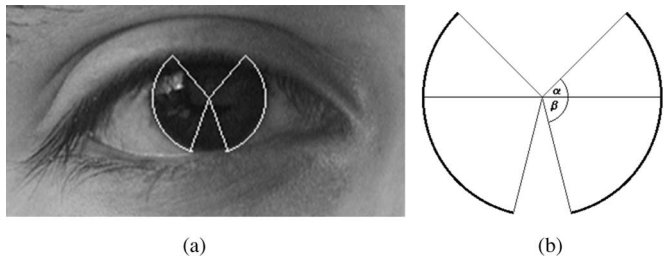

(a) (b)

Fig. 5. (a) Angles considered for the iris boundary detection. (b) Angles α and β measure the iris–sclera boundary free from eyelids occlusion.

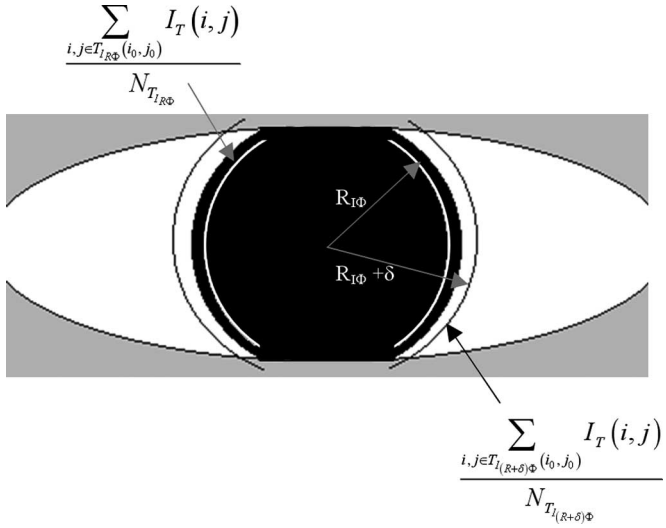

Fig. 6. Iris detection based on the ratio between two line integrals. Ratio will be maximum when the line integrals fall, one at each side of the iris–sclera boundary as illustrated.

$$R_{LI\Phi}(i_o,j_o) = \frac{\dfrac{\sum_{i,j\in T_{\mathrm{I}(\mathrm{R}+\delta)\Phi}(i_o,j_o)} I_T(i,j)}{N_{T_I\,(\mathrm{R}+\delta)\Phi}}}{\dfrac{\sum_{i,j\in T_{I\,R\Phi}(i_o,j_o)} I_T(i,j)}{N_{T_I\,R\Phi}}} \tag{7}$$

where $I_T(i,j)$ are the pixels along the $T_{IR\Phi}$, $N_{T_{I_{R\Phi}}}$ is the number of points that belong to $T_{IR\Phi}$ associated with radius $R_{I\Phi}$, and δ is the set in two pixels in the present study as shown in Fig. 6. According to (8), the radius $R_{I\Phi}$ is determined for three different sizes based on the detected face size b_{detected}. This face size is determined in the fine face detection stage

$$\begin{aligned} \text{Min } R_{I\phi} &= 0.11\left(\frac{\mathrm{b_{detected}}}{2} - 2\right) + 8 \\ \text{Max } R_{I\phi} &= \text{ Min } R_{I\phi} + 2. \end{aligned} \tag{8}$$

The location where the ratio between the line integrals is maximum is designated as the center of the iris and $2(R_{I\Phi}+\delta - 1)$ is the diameter of the iris. The iris size depends on the eyelid's opening. A search for a step change is performed in a line rotated in ϕ through the center of the pupil in $I_{er}(i,j)$.

D. Online Face and Iris Tracking in Video Sequences

The proposed method is applied to track the iris in real time. To allow real-time operation in video sequences, simplifications of the algorithm were performed. After processing the first frame, the video-tracking algorithm assumes the face fine location on the previous frame, as the coarse face detection for the present frame. Therefore, no coarse face detection is necessary after the first frame. Besides, since the face size does not change significantly from one frame to the next, only five values in steps of two pixels of the face semiaxis, and only three values of the rotation angles within $\pm$ 10° are used around the previously detected face size.

E. Database

The AR Face database [20] was used to build the generic templates. Since there is no database available for rotated faces, two were created for coronal axis rotation. Test_1 Database was created with five video sequences of five different individuals rotating their faces in the coronal axis. The number of frames in Test_1 Database varies from 286 to 297 in the five video sequences with a total of 1162 frames. Fig. 7 shows eight frames taken randomly from one video sequence. Test_2 Database was created with another set of five video sequences of five different individuals rotating their face in the coronal axis. The number of frames in Test_2 Database varies from 335 to 665 with a total of 2758 frames. All ten video sequences are in BMP format of 640×480 pixels and 24 bit/pixel color depth.

F. Performed Test

Two tests were performed for the proposed method.

TEST 1: The proposed method was compared to the original Maio–Maltoni's method [19] and to the Rowley's method [28], [29] for face detection. In the Rowley's method, the neural network was trained with faces extracted from the Purdue Database (1500 images) and with nonfaces (2650 images) of scenery as in [28] and [29]. As proposed in [17] and [29], to detect coronal rotated faces, the input image was rotated from -45° to 45° in step of 15° and presented as the input to the network. The best network output was selected for each rotated face. Since Maio–Maltoni's method does not consider face rotations, a version of our method (Method_R) restricted to frontal face detection with no rotation was produced. The unrestricted version of our method (Method_U) was also applied. Therefore, in Test 1 the Maio–Maltoni's method, Rowley's method, Method_R and the Method_U were applied to Test_1 Database.

TEST 2: Iris detection, face detection, and face size were determined applying Method_U to the Test_2 Database.

In both tests (TEST 1 and TEST 2) the results were assessed frame by frame.

III. Results

Fig. 8 shows the line integral values for different template rotations from -40° to 40°. Each curve represents a template at different rotation angles computing the line integral over the two images shown in Fig. 9. It can be observed that the line integral value is selective for the template rotation angle providing a maximum value when the rotation angle of the template and face coincide. In the case of Figs. 8 and 9, the rotation angles are -20° and 20° for each face, respectively.

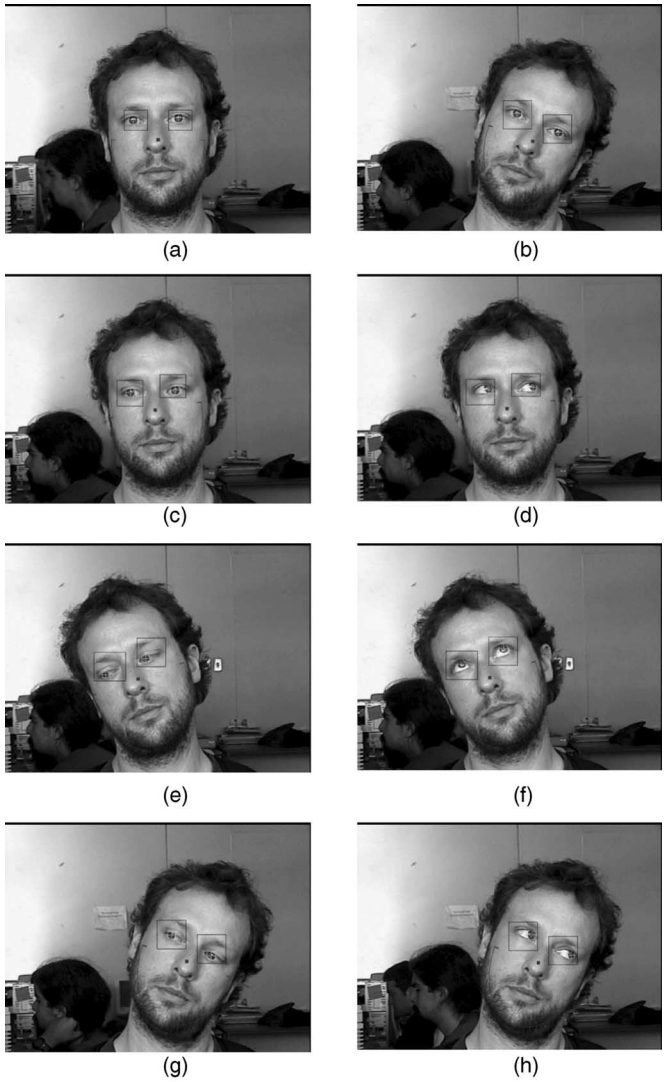

Fig. 7. Results of face detection, eye detection, and iris detection in eight random frames from one video sequence.

The method was assessed in two tests: TEST 1 compared the method to Maio–Maltoni's method and to Rowley's method for face detection in five video sequences with faces rotating in the coronal axis. Table I shows the video sequence number, the number of frames, and the percentage of frames with correct face detection for the Maio–Maltoni's method, Rowley's method, Method_R, and Method_U. It can be observed that the Maio–Maltoni's, method as well as Method_R behaves similarly without the template rotation. They fail to detect faces with rotations in the coronal axis with angles above 10°. Nevertheless, Method_U, with the template rotation, allows results above 99% in three of the five video sequences. The fourth video sequence reached 97.6% and the fifth 90.6%. In this last video sequence, the subject performed slight rotations in the sagital axis together with the coronal axis. The proposed method,

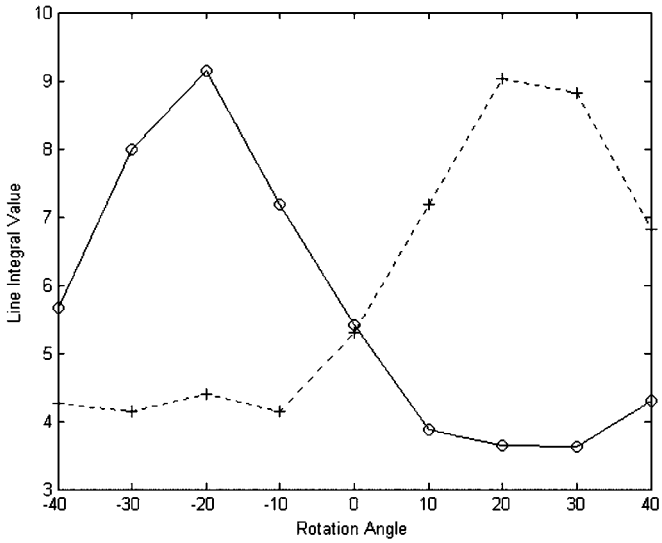

Fig. 8. Line integral value as a function of the coronal rotation angle. (○) Line integral for coronal rotated face in Fig. 9(a). (+) Line integral for coronal rotated face in Fig. 9(b).

(a)

(b)

Fig. 9. Images used to compute the line integral for different rotated templates. It also shows the results of face detection, eye region, and iris detection.

TABLE I
FACE DETECTION RESULTS IN TEST_1 DATABASE. COMPARISON AMONG MAIO–MALTONI'S METHOD, ROWLEY'S METHOD, METHOD_R, AND METHOD_U FOR FACE DETECTION. IT SHOWS THE VIDEO SEQUENCE, THE NUMBER OF FRAMES, AND THE CORRECT FACE DETECTION RATE

Video Sequence	Number of Frames	Correct Face Detection Rate (%)			
		Maio-Maltoni	Rowley	Method_R	Method_U
1	291	68.0	49.6	67.0	100.0
2	297	39.0	29.5	73.7	99.7
3	288	59.0	61.3	63.2	90.6
4	286	44.0	84.6	62.9	97.6
5	292	67.0	74.3	56.5	99.0

TABLE II
IRIS DETECTION, FACE DETECTION, AND FACE SIZE RESULTS IN TEST_2 DATABASE FOR THE METHOD_U. IT SHOWS THE VIDEO SEQUENCE, THE NUMBER OF FRAMES, THE CORRECT FACE DETECTION RATE, THE CORRECT IRIS DETECTION RATE, AND THE FACE SIZE DETECTION RATE

Video Sequence	Number of Frames	Correct Detection Rate (%)		
		Face Detection	Iris Detection	Face Size
1	556	98.2	96.0	99.9
2	335	100.0	100.0	100.0
3	629	100.0	99.9	99.9
4	573	100.0	100.0	100.0
5	665	100.0	99.7	100.0

Method_U, performed better than Rowley's method for rotated face detection. The poor performance of Rowley's method in video sequences 1 and 2 may be due to the ethnic type of the subjects that were less represented in the training data base.

Table II shows the video sequence number, the number of frames, the percentage of frames with correct face detection, the percentage of frames with correct iris detection, and the percentage of frames with correct face size estimation. It can be observed that face detection is 100% in four of the five video sequences. The fifth sequence scored 98.2% correct face detection. Iris detection is above 96% in all five video sequences with two above 99.7% and two 100%. Face size estimation is also above 99.9%.

Fig. 7 shows eight random frames from one video sequence detecting irises. The fine face detection and the region to detect the eyes (rectangle) are shown in black, and the iris center (cross) is shown in white. It is observed that the method detects iris position in different frames of the video sequence.

Processing time for online detection was 0.02 s, and it was measured on a PC Athlon XP 1.8 MHz, images 640×480 BMP RGB 24 bits format with no compression programming is in MS Visual C++ 5.0.

IV. CONCLUSION

A new noninvasive method was developed to track face and iris position in rotated faces in real time with a standard personal

computer. The method can follow head movements with no restrictions to the background, and it is based on anthropometrical templates built with information from the face and eye region from the individuals. The use of the face anthropometric information restricts the region of search, thus allowing real-time processing. It was shown that the line integral over the directional image computed with rotated templates was maximum when the face and template angle coincides. Therefore, the face rotation angle can be estimated by the line integral. This method was compared to that of Maio–Maltoni with similar results in nonrotated face detection. The method was also compared to Rowley's method for face detection, showing better results. Nevertheless, the proposed method goes further in allowing face rotations in the coronal axis and performing iris detection with high precision in real time. The method was assessed in five video sequences for face detection (TEST 1) and in another set of five video sequences for iris detection (TEST 2). The method was assessed rather extensively compared to other papers published in the literature, using 1162 frames in TEST 1 and 2758 frames in TEST 2. Results of correct face detection in TEST 1 were above 99% in three of the five video sequences. The fourth video sequence reached 97.6% and the fifth 90.6%. In the last video sequence, the subject performed slight rotations in the sagital axis together with the coronal axis. In TEST 2, the iris detection is above 96% in all five video sequences with two above 99.7% and two 100%. Face size estimation is also above 99.9%. The average processing time of our method was 0.02 s/frame. Thus, the proposed method can process frames at a rate near to 50 frames/s, and therefore, is applicable in real time in a standard personal computer.

V. Acknowledgment

The authors would like to thank their former graduate student Mr. A. Palma for his contributions in the online version of the method and in the implementation of Maio–Maltoni's method. They would also like to thank the Research Assistant J. Vallejos for his help in assessing the results and the anonymous reviewers for their useful comments to improve the manuscript.

References

[1] C. Chiang, W. Tai, M. Yang, Y. Huang, and C. Huang, "A novel method for detecting lips, eyes and faces in real time," *Real-Time Imag.*, vol. 9, pp. 277–287, Aug. 2003.

[2] J. G. Daugman, "High confidence visual recognition of persons by a test of statistical independence," *IEEE Trans. Pattern Anal. Mach. Intell.*, vol. 15, no. 11, pp. 1148–1161, 1993.

[3] J. G. Daugman, "How iris recognition works," *IEEE Trans. Circuits Syst. Video Technol.*, vol. 14, no. 1, pp. 21–30, Jan. 2004.

[4] J. Dowall, I. Pavlidis, and G. Bebis, "Face detection in the near-IR spectrum," *Image Vis. Comput.*, vol. 21, pp. 565–578, Jul. 2001.

[5] S. Eadie, "Improved method of measuring eye movements using limbus reflection technique," *Med. Bio. Eng. Comput.*, vol. 33, pp. 107–112, 1995.

[6] Y. Ebisawa, "Improved video-based eye-gaze detection method," *IEEE Trans. Instrum. Meas.*, vol. 47, no. 4, pp. 948–955, Aug. 1998.

[7] M. Eriksson and N. P. Papanikolopoulos, "Driver fatigue: A vision-based approach to automatic diagnosis," *Transp. Res. C*, vol. 9, pp. 399–413, 2001.

[8] J. A. Horne and L. A. Reyner, "Driver sleepiness," *J. Sleep Res.*, vol. 2, pp. 23–29, 1995.

[9] J. P. Ivins, J. Porrill, and J. P. Frisby, "Deformable model of the human iris for measuring ocular torsion from video images," *Inst. Electr. Eng. Proc. Vis. Image Signal Process.*, vol. 145, no. 3, pp. 213–220, Jun. 1998.

[10] Q. Ji, "3D face pose estimation and tracking from a monocular camera," *Image Vis. Comput.*, vol. 20, pp. 499–511, May 2002.

[11] M. Jones and J. Rehg, "Statistical color models with application to skin detection," *Int. J. Comput. Vis.*, vol. 46, pp. 81–96, Jan. 2002.

[12] M. Jones and P. Viola, "Fast multiview face detection," Mitsubishi Elect. Res. Lab., Tech. Rep., TR2003-96 Jul. 2003.

[13] J. Kim, K. R. Park, J. J. Lee, and S. R. LeClair, "Intelligent process control via gaze detection technology," *Eng. Appl. Artif. Intell.*, vol. 13, pp. 577–587, Aug. 2000.

[14] J. R. LaCourse and F. C. Hludik, Jr., "An eye movement communication-control system for the disable," *IEEE Trans. Biomed. Eng.*, vol. 37, no. 12, pp. 1215–1220, Dec. 1990.

[15] M. W. Lee and S. Ranganath, "Pose-invariant face recognition using 3D deformable model," *Pattern Recognit.*, vol. 36, pp. 1835–1846, Aug. 2003.

[16] Y. Li, X. Qi, and Y. Wang, "Eye detection by using fuzzy template matching and feature-parameter-based judgement," *Pattern Recognit. Lett.*, vol. 22, pp. 1111–1124, 2001.

[17] C. Lin and K. Fan, "Triangle-based approach to the detection of human face," *Pattern Recognit.*, vol. 34, no. 6, pp. 1271–1284, 2001.

[18] C. Lin and K. Fan, "Pose classification of human faces by weighting mask function approach," *Pattern Recognit. Lett.*, vol. 24, pp. 1857–1869, Aug. 2003.

[19] D. Maio and D. Maltoni, "Real time face location on gray scale static images," *Pattern Recognit.*, vol. 33, pp. 1525–1539, Sep. 2000.

[20] A. Martínez and R. Benavente, "The AR face database," Univ. Purdue, CVC Tech. Rep. 24, 1998, [Online]. Available: http://rv11.ecn.purdue.edu/∼ aleix/aleix_face_DB.html.

[21] K. S. Park and C. J. Lim, "A simple vision-based tracking method for eye-controlled human/computer interface," *Int. J. Human.-Comput. Studies.*, vol. 54, pp. 319–332, Mar. 2001.

[22] C. A. Perez, A. Palma, C. A. Holzmann, and C. Peña, "Face and eye tracking algorithm based on digital image processing," in *Proc. 2001 IEEE Int. Conf. Syst., Man, Cybern.,* Tucson, AZ, Oct. 2001, vol. 2, no. 7–10, pp. 1178–1183.

[23] C. A. Perez, C. Peña, C. A. Holzmann, and C. M. Held, "Design of a virtual keyboard based on iris tracking," in *Proc. 2nd Joint Conf. IEEE/EMBS BMES*, Houston, TX, Oct. 2002, vol. 3, no. 23–26, pp. 2428–2429.

[24] C. A. Perez, C. A. Salinas, P. A. Estévez, and P. Valenzuela, "Genetic design of biologically inspired receptive fields for neural pattern recognition," *IEEE Trans. Syst., Man, Cybern. B*, vol. 33, no. 2, pp. 258–270, Apr. 2003.

[25] C. A. Perez, G. D. González, L. E. Medina, and F. J. Galdames, "Linear vs. nonlinear neural modeling for 2-D pattern recognition,," *IEEE Trans. Syst., Man, Cybern. A*, vol. 35, no. 6, pp. 955–964, Nov. 2005.

[26] C. A. Perez, V. A. Lazcano, P. A. Estévez, and C. M. Held, "Real-time iris detection on rotated faces," in *Proc. SPIE Optomechatronics Syst. IV(RB5),* Providence, RI, Oct. 2003, vol. 5264, pp. 42–53.

[27] C. A. Perez, V. A. Lazcano, P. A. Estévez, and C. M. Held, "Real-time iris detection on faces with coronal axis rotation," in *Proc. 2004 IEEE Int. Conf. Syst., Man, Cybern.*, Hague, The Netherlands, Oct. 2004, vol. 7, no. 10–13, pp. 6389–6394.

[28] H. Rowley, S. Ahuja, and T. Kanade, "Neural network-based face detection," *IEEE Trans. Pattern Anal. Mach. Intell.*, vol. 20, no. 1, pp. 23–38, Jan. 1998.

[29] H. Rowley, S. Ahuja, and T. Kanade, "Rotation invariant neural network-based face detection," in *Proc. 1998 IEEE Comput. Soc. Conf. Comput. Vis. Pattern Recognit. (CVPR)*, Santa Barbara, CA, Jun. 1998, pp. 38–44.

[30] S. Sirohey, A. Rosenfeld, and Z. Duric, "A method of detecting and tracking irises and eyelids in video," *Pattern Recognit.*, vol. 35, pp. 1389–1401, Jun. 2002.

[31] J. G. Wang and E. Sung, "Study on eye gaze estimation," *IEEE Trans. Syst., Man, Cybern. B*, vol. 32, no. 3, pp. 332–350, Jun. 2002.

[32] M. Yang, J. Kriegman, and N. Ahuja, "Detecting faces in images: A survey," *IEEE Trans. Pattern Anal. Mach. Intell.*, vol. 24, no. 1, pp. 34–58, Jan. 2002.

[33] Z. Zhu and Q. Ji, "Robust real-time eye detection and tracking under variable lighting conditions and various face orientations," *Comput. Vis. Image Understanding*, vol. 98, pp. 124–154, 2005.

Claudio A. Perez (M'90–SM'04) received the B.S. and P.E. degrees in electrical engineering and the M.S. degree in biomedical engineering, all from the University of Chile, Santiago, and the Ph.D. degree from The Ohio State University (OSU), Columbus, in 1980, 1985, and 1991, respectively.

Currently, he is a Faculty Member in the Department of Electrical Engineering, the University of Chile where he was the Chairman of the department from 2003 to 2006. In 1991, he received a Fellowship for Chilean Scientists from Fundacion Andes. He was an invited speaker at the OSU and was a part of the Fulbright faculty exchange with the University of California, Berkeley. His research interests include computational vision, new models for pattern recognition, and man–machine interfaces.

Dr. Perez is a member of the IEEE Systems, Man, and Cybernetics Society, IEEE Biomedical Engineering Society, IEEE Neural Network Society, Pattern Recognition Society, International Society for Optical Engineers, Sigma-Xi, and the OSU Alumni Association. He was a Fulbright student at OSU, and in 1990, he was a Presidential Fellow and received a Graduate Student Alumnni Research Award from OSU.

Vanel A. Lazcano received the B.S. and P.E. degree in electrical engineering from the University of Chile, Santiago, in 2004. He is working toward the M.S. degree in electrical engineering at the University of Chile.

He is working as a Research Staff in FONDEF project D04I1256 on face detection and recognition at the University of Chile. His research interests include face and iris detection, face recognition, and industrial applications˜of image processing systems.

Pablo A. Estévez (M'98–SM'04) received the B.S. and P.E. degrees in electrical engineering from the Universidad de Chile, Santiago, and the M.S. and Ph.D. degrees from the University of Tokyo, Tokyo, Japan, in 1978, 1981, 1992, and 1995, respectively. He received the Mombusho Fellowship to pursue his Ph.D. degree at the University of Tokyo.

Currently, he is an Associate Professor in the Electrical Engineering Department, University of Chile, where he is also the Chairman of the department. He is also a Distinguished Lecturer with the IEEE Computational Intelligence Society. He has been an Invited Researcher at the Communication Science Laboratory, NTT-Kyoto, Japan, and at the Ecole Normale Superieure de Lyon, France. His research interests include the application of neural networks and evolutionary algorithms to pattern recognition and biomedical issues.